Unsteady Characteristics of Turbomachinery—Interface between Vibration and Fluid Mechanics

H. OHASHI
Department of Mechanical Engineering
University of Tokyo
Hongo, Bunkyo-ku, Tokyo 113, Japan

INTRODUCTION

A turbomachine, a turbopump for example, must achieve a given pressure rise at its design flow rate with the highest possible efficiency. Beyond these performance requirements at design point, a good turbopump must have also such favorable characteristics as less performance deterioration at the off-design point, especially at partial flow rate and quiet operation with less noise and vibration, etc. These are all performance qualifications at steady operating conditions and most of the R&D activities on turbomachinery have been devoted to the improvement of steady performances.

Turbomachines are also exposed to unsteady operating conditions. The most frequent unsteady operation takes place during the transients such as start-up and shut-down or quick closure and opening of valves. They are initiated however by an intentional maneuvering and last only for a short period. Dynamic performances of turbopumps during such short transients have been studied for various cases from the interest in precise performance prediction [Ref. 1-3].

Other unsteady operations are usually caused by unexpected reasons, mostly due to the instability of the hydraulic system consisting of pipings and turbomachines. A typical example is the surging of a pumping system. Once the surging occurs, the flow rate and pressure rise of the turbopump oscillate quite violently and it results in an emergency shut-down or failure of the system. POGO (self-excited longitudinal oscillation of liquid propellant rocket) is also caused by the dynamic instability of combined structure and hydraulic systems.

For the stability analysis of a pumping system, the dynamic behavior of all system elements such as pipings, valves, pumps, etc. must be known. Pumps supply all flow energy to the system and thus play an active and determining role for the system dynamics. In spite of this significance we find even in the current system analyses that the turbopump performance during unsteady operation is simply substituted by the steady performance. The excuse of vibration specialists for this a priori assumption is always the lack of information on the unsteady performances. We admit that the vibration specialists, who conduct such system analyses, are not directly responsible for this situation, because the problem of unsteady performance of turbomachinery is quite a specified research theme beyond their expertise. This problem is surely worth challenging for fluids specialists. The relation between pump performance and the stability of pumping systems was summarized in the 1980 Freeman Scholar Lecture by Greitzer [Ref. 4].

We see here an unbalance of knowledge. A turbomachine, whose flow has been fully analyzed and verified to the utmost detail in the R&D process, s treated quite simply in the vibration analysis. If once instability occurs against prediction due to an improper assumption, the whole turbomachine with a marvelous performance could become just useless.

A similar situation can be seen in the analyses of rotordynamic stability of a rotating shaft. The shaft of a turbopump, for example, consists of many elements such as bearings, seals, bushes, impellers, etc., which rotate and whirl with the shaft together. For the analysis of this shaft system, the fluid forces on these elements during vibration must be known. Many studies have been carried on the fluid forces of bearings and annular seals but little is known about those of impellers. In the current practice of rotordynamics, a presumed amount of apparent mass is merely added to each impeller. This assumption is also unbelievably simple compared to the precise analysis of impeller flow aimed for the performance improvement. The study of fluid forces on vibrating impellers seems also beyond the expertise of vibration specialists.

Excellent fluid dynamic performance of turbomachines can be exploited only when they operate vibration-free. Therefore, the tasks to provide vibration specialists with the accurate information on the dynamic behavior of turbomachines are as important as the ones to improve their performance itself. In the present paper, two examples of such interfaces between vibration and fluid mechanics are introduced, one on the unsteady performance of turbopumps and another on the fluid forces on a whirling centrifugal impeller.

Fluid phenomena are non-linear in their nature. Pressure losses, stagnation pressure, lift and drag; they are all proportional to the square of velocity. In the vibration analysis of a complicated system, however, the dynamic characteristics of system elements are usually assumed to be linear. It is quite an understandable simplification in practice, when we consider the complexity of the calculation needed for the analysis. In many cases information on unsteady fluid phenomena, which is perfectly correct and consistent from the viewpoint of fluid mechanics, has not been used in the relevant vibration analysis, since the result was not presented in a directly applicable form. Fluids specialists should rearrange their materials to such an extent that they can be readily applied in the vibration analysis. A good interface between vibration and fluid mechanics can be established, only when we understand well what they need.

DYNAMIC PERFORMANCE OF TURBOPUMPS

Pump Performance for Fluctuating Flow Rate

Let us consider a very simple pumping system as illustrated in Fig. 1, in which a turbopump feeds water from a low pressure to a high pressure reservoir. The hydraulic performance of a turbopump at a constant rotational speed is expressed usually by a curve like the one in Fig. 2, which indicates the relation between flow rate and pressure rise (P-Q curve). When the system is stable, the pump operates at point A on its performance curve, which is the crossing point of performance and resistance curves.

When the pumping system becomes unstable for some reason, mostly due to the positive slope of P-Q curve at the operating point or to the inception of cavities in the system, the discharge of the pump begins to oscillate. If the fluctuation is sufficiently slow, the instantaneous pressure rise of the pump varies obviously along the steady P-Q curve. As the fluc-

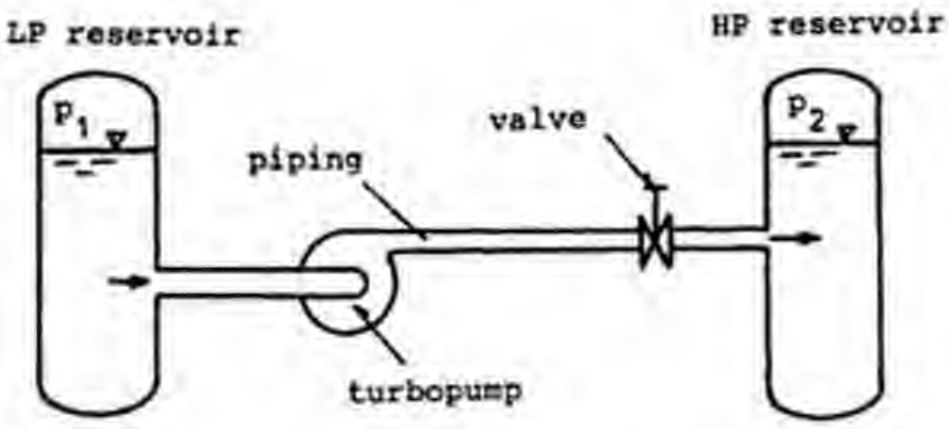

Fig. 1 Pumping system

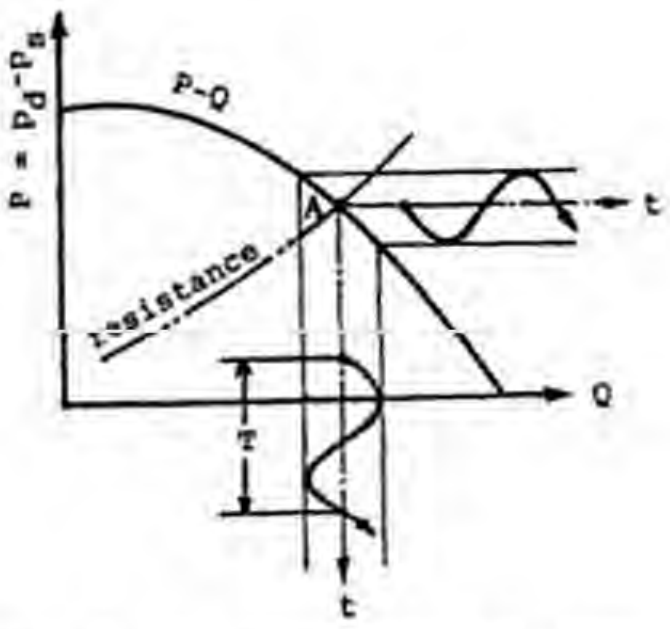

Fig. 2 Quasi-steady performance

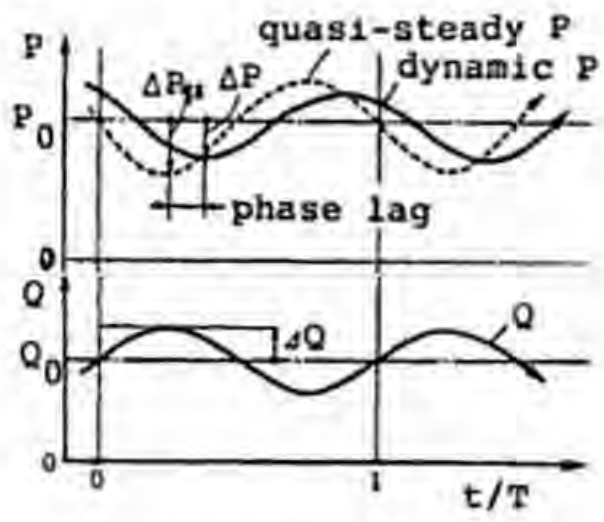

Fig. 3 Dynamic and quasi-steady pressure rise

tuation frequency increases, the time lag of the internal flow gives rise to a delay of the pressure rise of the pump, thus resulting in the deviation of dynamic P-Q curve from the one at steady condition. Fig. 3 illustrates the possible deviation of the dynamic pressure rise from the steady one for the same flow fluctuation. The problem of dynamic performance is hence to make clear; 1) the critical frequency beyond which the quasi-steady assumption becomes inadequate and 2) the deviation of dynamic performance from the quasi-steady one when the frequency limit is surpassed.

Pressure Rise by Pumping Action

In the case of unsteady operation, special attention must be paid to the meaning of total pressure rise P of the pump, which is defined usually as the increase of the total pressure from suction to delivery generated by the pumping action. In the case of steady flow rate, all total pressure rise is obviously generated by the pumping action of rotating impellers. In the case of unsteady flow rate, however, a part of the total pressure difference is caused by the inertia of water contained in the pump impeller and casing. This part is called total pressure difference by conduit effect, P_c, and is calculated by the equation

$$P_c = -\rho (L_{eq}/A_0)(dQ/dt) \qquad \text{.....(1)}$$

where A_0 is the reference cross sectional area, L_{eq} the equivalent length of the pump. In order to determine equivalent length, the flow passage of the pump from suction to delivery port must be transformed at first to a

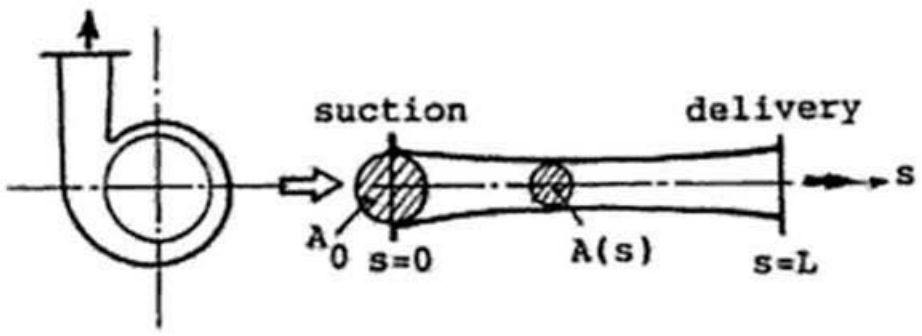

Fig. 4 Equivalent length

one-dimensional pipe with variable cross section A(s) as shown in Fig. 4, and then to an equivalent pipe of length L_{eq} with reference cross section A_0, where L_{eq} is given by the relation

$$L_{eq} = \int_{s=0}^{L} (A_0/A(s))\, ds \qquad \text{.....(2)}$$

The true total pressure rise by pumping action during unsteady operation, P, can be calculated from measured total pressure rise, P_m, and apparent total pressure difference by conduit effect, P_c, by

$$P = P_m - P_c \qquad \text{.....(3)}$$

The total pressure rise indicated in Fig. 3 is, of course, the true one excluding the pressure difference due to the conduit effect. From the viewpoint of fluid mechanics, the main interest consists in the dynamic behavior of this true pressure rise, i.e. pumping action at fluctuating flow rate. From the viewpoint of vibration analysis, however, the necessary information is the dynamic behavior of the whole pump including also conduit effect. This is an example of the interest gap, often seen in the study of unsteady flow phenomena.

It is hardly possible to determine the equivalent length in an exact meaning. This is especially the case when the pump is equipped with a volute casing, in which the length of stream lines is different depending on the angular location of discharge into the volute. This fact implies that the equivalent length of volute is a function of fluctuation frequency in such manner that the higher the frequency, the shorter the equivalent length [Ref. 5].

Equivalent length can be also estimated experimentally. For this purpose the flow rate is forced to oscillate by an external device while the pump shaft is kept standstill. The measured flow rate acceleration dQ/dt and total pressure difference, P_c, give rise to an equivalent length by Eq.(1). This method involves also an uncertain factor, because the length of the absolute stream line in the impeller is different depending on whether it rotates or stands still.

Lag of Pressure Rise

The reason why the pressure rise of an impeller cannot respond quickly enough to the instantaneous flow condition and allows a certain time lag, is divided into three major factors:

1) Potential lag Potential lag is defined as the one which occurs even under the assumption of incompressible potential flow. A typical example can be seen in the lag of circulation and lift growth of an isolated

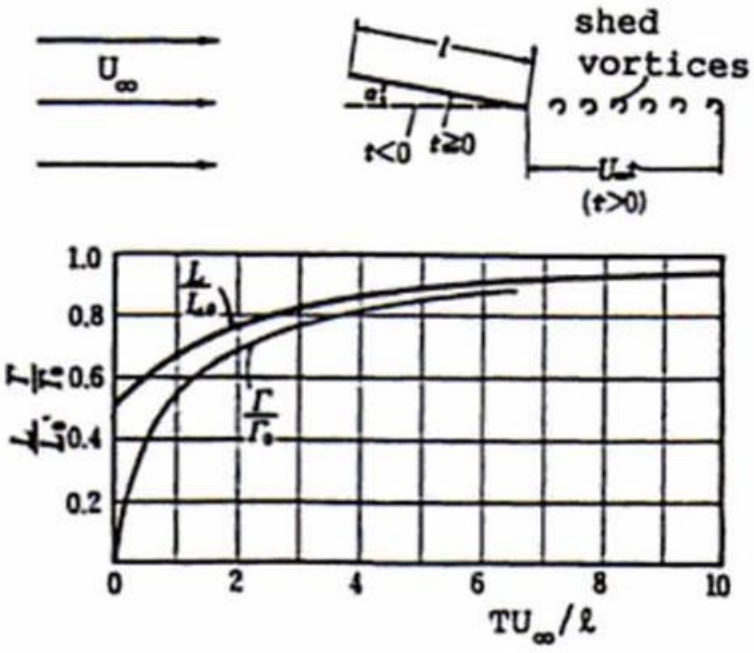

Fig. 5 Lag of circulation and lift

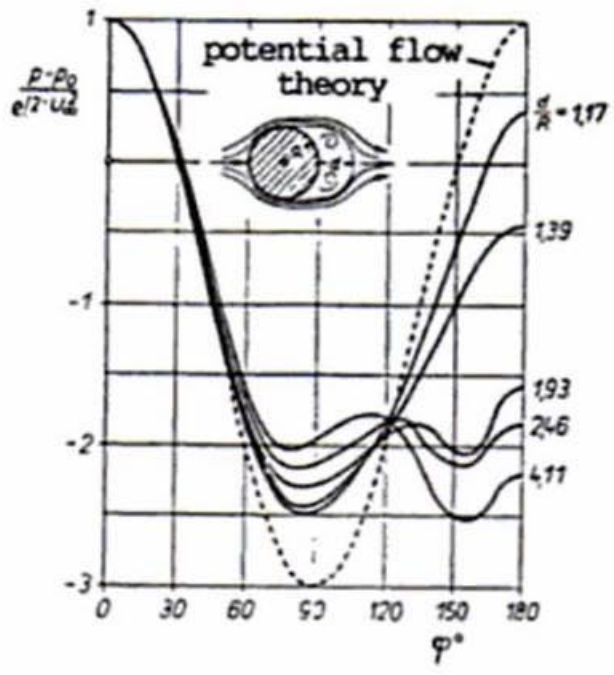

Fig. 6 Lag of separation growth

airfoil when it changes its attack angle stepwise from zero to a finite value at t = 0. Fig. 5 shows the growth of circulation and lift calculated by Wagner [Ref. 6], where U_∞ is uniform velocity, ℓ chord length, Γ_0 and L_0 asymptotic circulation and lift, respectively. As seen from this example, the time lag of potential flow in lift and circulation generation is about 2 in non-dimensional time unit, tU_∞/ℓ. The essential reason of this time lag consists in the fact that counter-vortices are shed from the trailing edge so as to suppress sudden growth of airfoil circulation. It takes a definite time for the shed vortices till they are carried so far away that they lose their suppressive effect.

From the above consideration it is clear that the potential lag is proportional to chord length and inversely to flow velocity.

2) Viscous lag It requires a certain time for the boundary layer to grow its thickness and eventually to develop into a separated region. Fig. 6 illustrates the evolution of pressure distribution around a circular cylinder after it starts moving suddenly from standstill. The parameter in the figure is displacement d normalized by cylinder radius. Immediately after the start the pressure distribution is very close to the one calculated by the potential theory and it proves that no separation region does exist at this moment. Only after the cylinder moves more than twice the diameter, the pressure distribution becomes similar to the steady one, which features a large separated region behind the cylinder. It is noteworthy that the lag time due to viscous effect is also about 2x(representative length)/ (representative velocity) as in the case of potential lag.

In the dynamic performance of turbopumps, potential lag seems to play an essential role, since the pressure rise of pumps is primarily achieved by the lift of impeller blades.

3) Compressibility lag In pumps handling two-phase flow and cavitating flow, the compliance of cavities causes a definite lag. For the dynamic characteristics of cavitating pumps and inducers, this lag is the major concern [Ref. 7-9].

Dynamic Characteristics Represented by Transfer Matrix

When the pressure and flow rate of a turbopump at suction, p_1 and Q_1, fluctuate, the pressure and flow rate at delivery, p_2 and Q_2, vary accordingly. If we assume here a linear relation that the pressure and flow rate

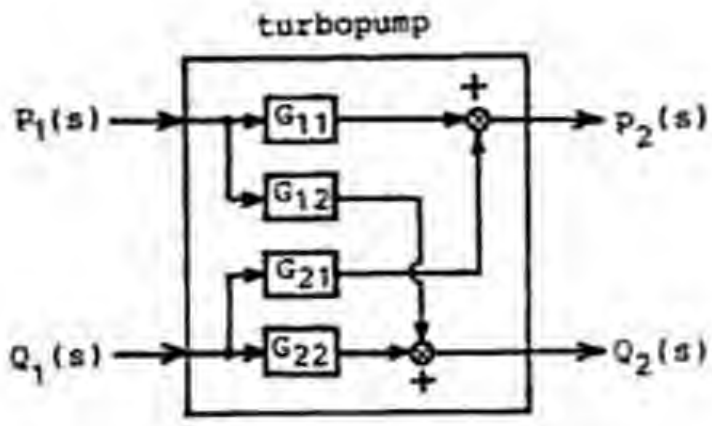

Fig. 7 Transfer matrix

fluctuation at suction induce the fluctuation of delivery conditions independently, the both effects can be superimposed (see Fig. 7). The variables at suction and delivery are then expressed by the next equation.

$$\begin{bmatrix} p_2(s) \\ Q_2(s) \end{bmatrix} = \begin{bmatrix} G_{11}(s) & G_{12}(s) \\ G_{21}(s) & G_{22}(s) \end{bmatrix} \cdot \begin{bmatrix} p_1(s) \\ Q_1(s) \end{bmatrix} \qquad \text{.....(4)}$$

where four variables $p_1(s)$, $Q_1(s)$, $p_2(s)$, $Q_2(s)$ are the Laplace transformed functions of fluctuating variables $p_1(t)$,. in the time domain. Four transfer functions $G_{11}(s)$,... correlate the variables at suction and delivery. The set of these four transfer functions is called transfer matrix of the turbopump.

When we substitute s in the transfer functions by $j\omega$ (j is imaginary unit and ω angular speed), they represent frequency response functions which describe the amplitude and phase relation of input and output.

Although the real flow phenomena in turbopumps are not exactly linear as assumed in the above, their dynamic characteristics are expressed usually by Eq.(4) for the convenience of system analyses.

Dynamic Performance of a Low-Pressure Non-Cavitating Pump

When a turbopump operates cavitation-free under a sufficient boost pressure and the pump casing is stiff enough, the whole flow phenomena can be considered as incompressible. In this case the flow rate at suction and delivery are always the same and the pressure rise is not affected by the level of the inlet pressure. It leads to the consequence that $G_{11}=1$, $G_{21}=0$ and $G_{22}=1$. The interest in this case is to determine G_{12}, which is called impedance of the pump.

The pressure difference between delivery and suction is caused partly by pumping action and partly by conduit effect as mentioned above. If we assume that the dynamic pressure rise and equivalent length of the pump remain unchanged independent of fluctuation frequency, the pump impedance can be expressed by

$$G_{12} = -(R_p + Ls) \qquad \text{.....(5)}$$

where $R_p = -\partial P/\partial Q$ (pump resistance) and $L = \rho L_{eq}/A_0$ (inertance). The interest of dynamic study consists in the verification of this simple description.

Fig. 8 illustrates a test setup, by which dynamic characteristics of a turbopump was measured for the first time [Ref. 10, 11]. A small low-pressure centrifugal pump with 50 mm suction diameter was tested for the flow fluctuation up to 10% of mean discharge.

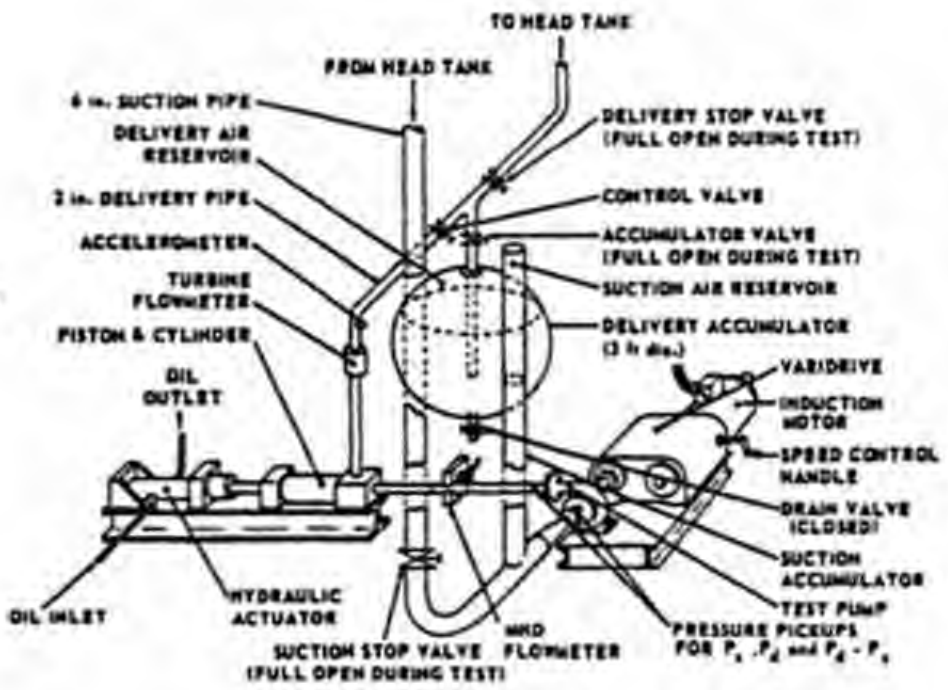

Fig. 8 Test setup

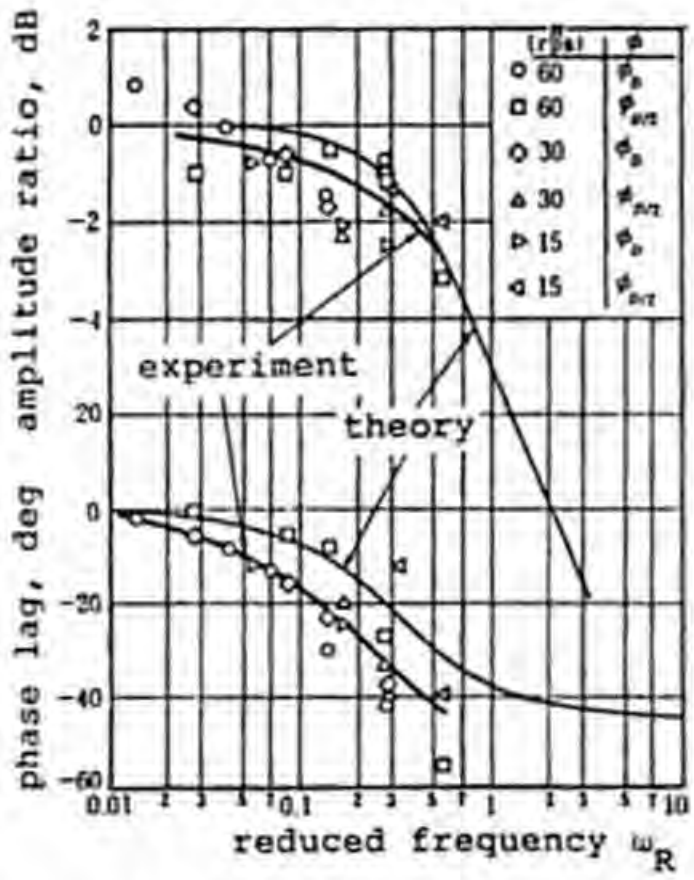

Fig. 9 Pressure rise response

The result is summarized in Fig. 9, in which the phase lag (in degree) and amplitude ratio (in decibel) of measured dynamic resistance to the quasi-steady resistance R_p are plotted against reduced frequency of impeller blade, ω_R. This relation indicates also the phase and amplitude relation of dynamic and steady pressure rise illustrated in Fig. 3.

Reduced frequency of impeller is defined by $\omega_R = (\cos \lambda_R / N_R \phi) \times (f/n)$, where λ_R and N_R are stagger angle and number of impeller blades, ϕ flow coefficient, f fluctuation frequency and n rotational speed. Though the definition is complicated, its physical meaning is exactly the same as that of an isolated airfoil. Data at three different rotational speeds and two flow coefficients (design and half-design flow) are plotted together. Thin solid lines in the figure indicate an analytical result derived from the unsteady potential flow around the cascade. Pressure rise response depends, of course, on the geometries of both impeller and guide vanes (rotor and stator).

From the above result, the following can be interpreted:

1) The critical condition, beyond which quasi-steady assumption begins to fail, is expressed by $\omega_R = 0.1$. Critical fluctuation frequency f_{cr} can be calculated therefore by

$$f_{cr} = 0.1 \times (N_R \phi / \cos \lambda_R)\, n \qquad \text{.....(6)}$$

For a typical centrifugal impeller with $N_R = 8$, $\phi = 0.1$ and $\lambda_R = 25°$, critical frequency is about $f_{cr} = 0.1\, n$, and this can be used as a rule of thumb for common turbopumps.

2) When frequency exceeds critical value, phase lag increases and amplitude ratio of pressure rise decreases as seen in the figure. Though the measured dynamic response of Fig. 9 cannot be expressed by a simple transfer function in an exact sense, the response can be approximated by the first order lag with a time constant of $T = 1/2\pi f_{cr}$. Therefore the pump impedance is better given by

$$G_{12}(s) = -R_p/(1 + Ts) - Ls \qquad \text{.....(7)}$$

3) The above result applies only to the case of small fluctuation without cavity formation. If once cavitation occurs under severe pressure fluctuation, the linear relation between flow and pressure fluctuation deteriorates badly and fractional harmonics such as f/2, f/3 appears in the pressure fluctuation.

Dynamic Performance of a High-Pressure Non-cavitating Multistage Pump

Most of the instability of pumping systems are caused by operating pumps at partial flow, where the slope of P-Q curve is positive. In any system instability accompanied by a severe oscillation of flow and pressure, there must be a definite source or mechanism, which supplies the excitation energy continuously to the fluid. The positive slope of P-Q curve is most understandable and popular mechanism of such an energy supply.

In some cases, especially in high pressure hydraulic system with high-speed turbopumps, system instability occurs even when the pump operates at negative slope region and cavitation-free. During the search for the excitation source of such instability, there arose a suspicion whether the negative slope of the characteristics could be maintained also for unsteady operations. The dynamic performance test introduced in this section was conducted to answer the above question [Ref. 12, 13].

As expected from Eq.(6) the critical frequency of a high-speed turbopump is correspondingly higher. It means that the the pump must be tested up to higher frequency range. At high frequency or when the wave length $\lambda=a/f$ (a=acoustic velocity) becomes comparable to the equivalent length of the pump, the compressibility of the liquid is no more negligible, even though there is no cavity at all. In this study, therefore, all four elements of the transfer matrix, G_{11} to G_{22}, are to be determined by the experiment.

The specification of prototype pump, 10 stage centrifugal volute pump, is listed in Table 1. The test was conducted for the first three stages by the test rig illustrated in Fig. 10. The fluctuation of flow rate is generated by an exciter piston attached to the suction line. The fluctuation frequency is adjusted between 2 and 20 Hz and the fluctuations of pressure and flow rate at suction and delivery are recorded at each frequency for two different piping conditions. For a pump of very small compressibility, as it is the case of the present one, G_{11} and G_{22} are very close to unity and the attention is mainly paid to the character of G_{12} and G_{21}.

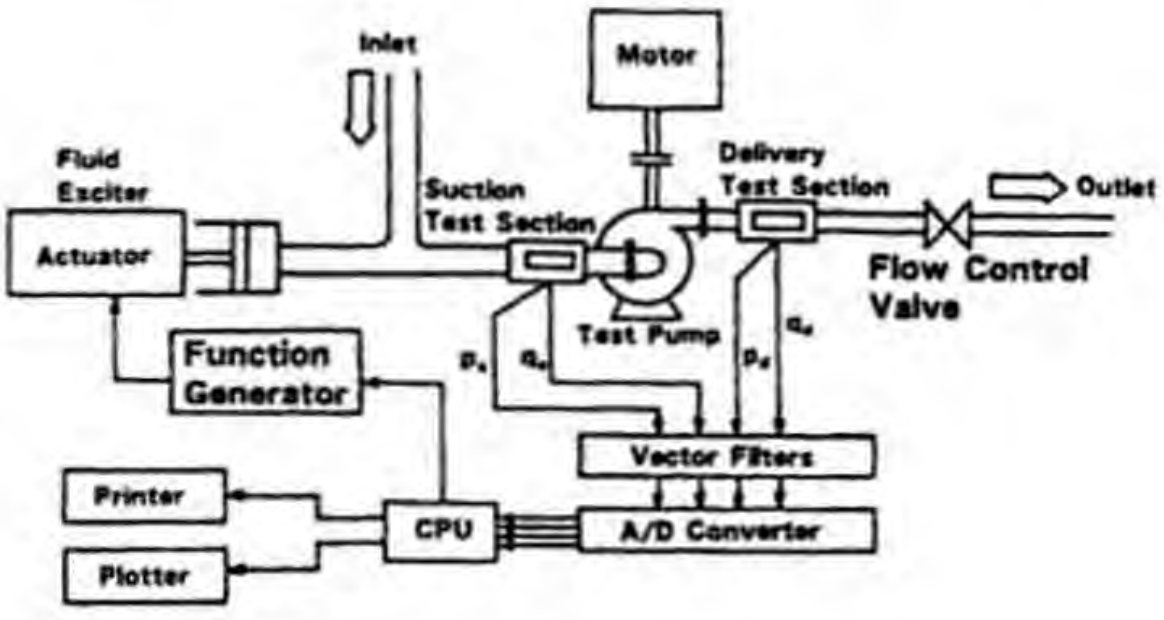

Fig. 10 Test system for high-pressure pump

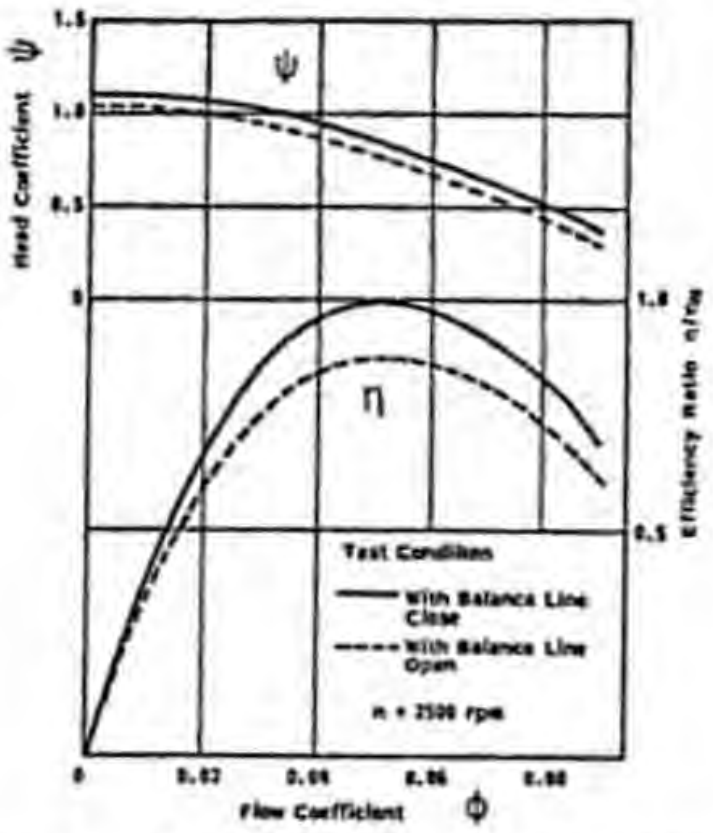

Fig. 11 Quasi-steady characteristics

Table 1 Specification

Pump Head	H = 1000 m
Flow Rate	Q = 159 m^3/h
Rotating Speed	n = 3000 rpm
No. of Stage	10

Fig. 11 shows the steady state characteristics of the test pump. It is clear that the slope of the P-Q curve is negative over the entire flow range and no instability could be induced as far as steady characteristics are concerned. In Fig. 12 (a) the measured resistance, i.e. the real part of G_{12}, is plotted against frequency for various mean flow rate, while (b) for various rotational speed.

A peculiar result is observed from the figures that a negative resistance, equivalent to the positive slope of P-Q curve, appears at low frequency range of 2 to 6 Hz, when the pump operates at partial flow rate less than 20 % of design flow and this feature becomes stronger as rotational speed increases. If the piping system has a resonant frequency in this frequency range, a system instability can be incurred, unless there is a sufficient damping in the system to suppress the excitation caused by the dynamic pump characteristics. The flow mechanism of why pump resistance turns to negative at certain unsteady conditions has not been clarified at all and remains an interesting question of unsteady characteristics.

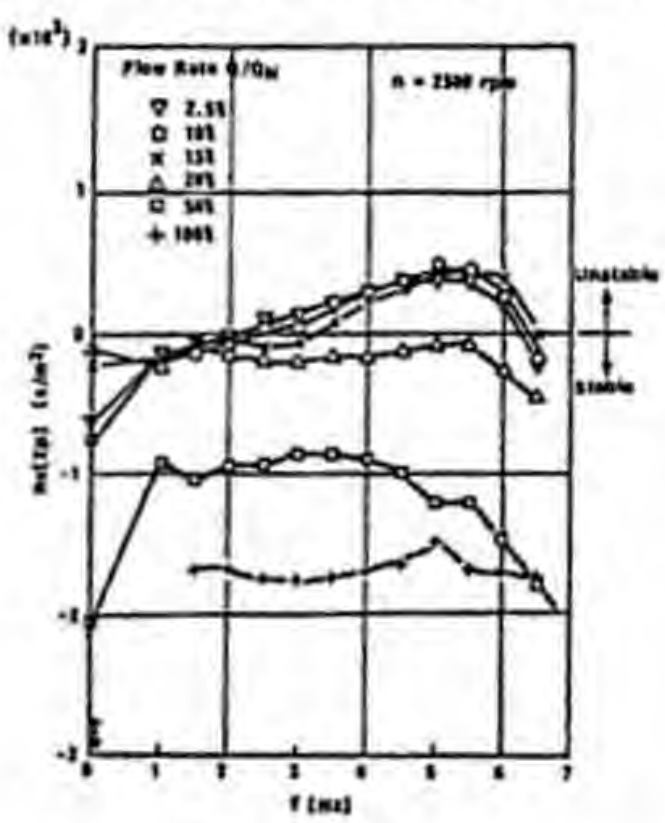

(a) Influence of flow rate

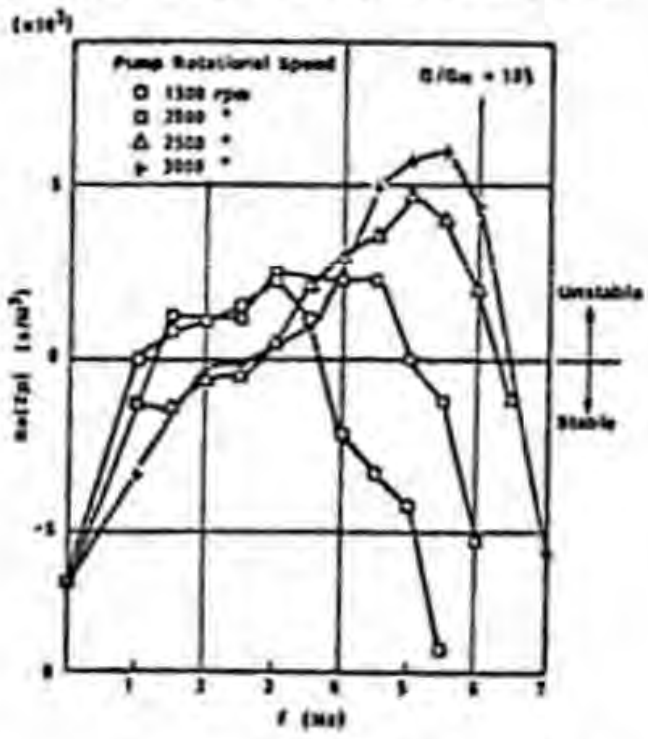

(b) Influence of rotaional speed

Fig. 12 Pump resistance

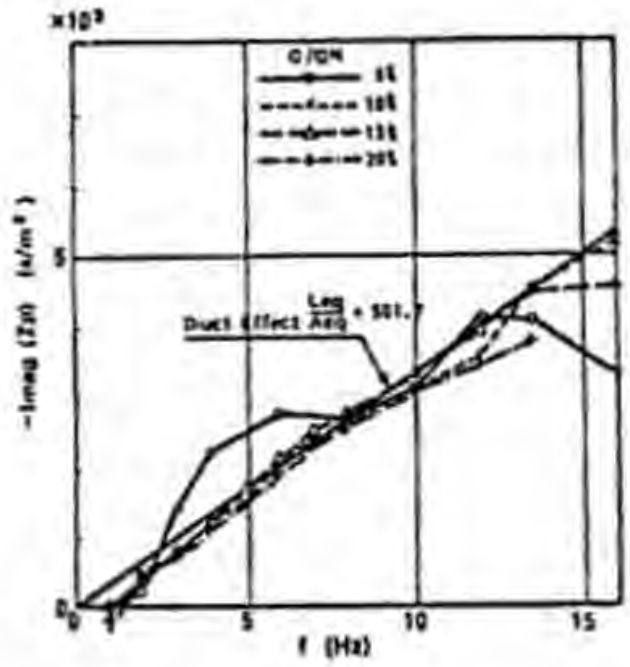

Fig. 13 Pump inertance

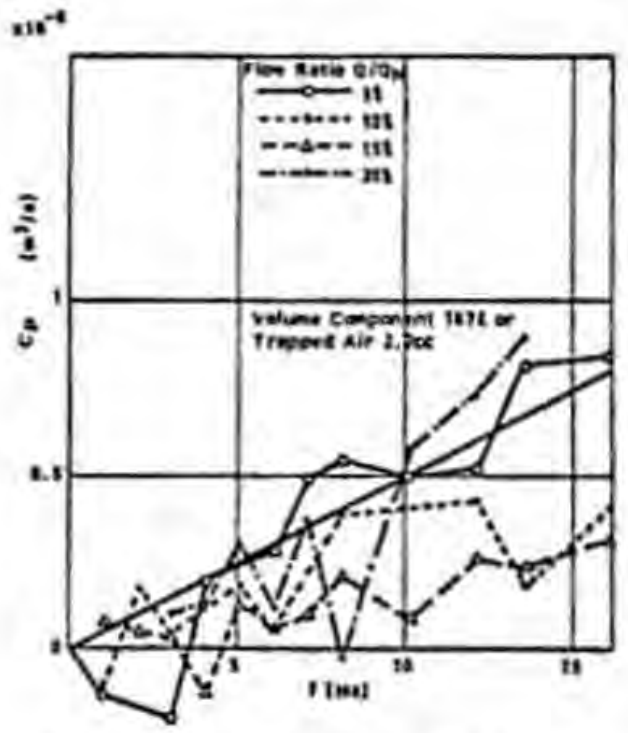

Fig. 14 Pump compliance

Fig. 13 shows the inertance, imaginary part of G_{12}, of the test pump. From the slope of this inertance curve, the equivalent length of the pump can be estimated. In Fig. 14 the compliance, imaginary part of G_{21}, is plotted for frequency. This compliance corresponds to the bulk elasticity of about 170 litre of water or to 2.2 cm^3 of air cavity. Elasticity of the pump casing, elasticity of water contained in the casing, tiny cavities trapped in bushings, seals and balancing device add up to a resultant compliance of the pump.

As seen from the above example, dynamic characteristics of turbopumps have a significant meaning for the system stability. Extensive studies are further expected for a better understanding of unsteady characteristics. The dynamic characteristics of cavitating pumps and inducers are also very important and interesting field of study, though they are not introduced in detail in the present paper (see Ref. 4).

FLUID FORCE ON WHIRLING IMPELLER

Fluid Forces and Rotordynamics

Besides the instability of hydraulic systems, vibration of rotating shaft is another cause of major trouble which high-speed, high-performance turbomachines encounter during the R&D period and also at the plant site. For high-speed multistage centrifugal pumps and compressors, whose rotors are usually less rigid than in other machines, the prediction of rotordynamic stability has a special importance.

For the rotordynamic stability analysis of a turbopump, for example, it is necessary to estimate the fluid dynamic forces acting on each element of the rotor such as journal bearing, wear ring, throttle bushing, balance piston and centrifugal impeller. Many studies have been done for fluid forces on bearings and annular seals [Ref. 14-16] but few for forces on impellers, even though they are the principal components of the rotor.

The fluid forces of the interest in the rotordynamic analyses are not the steady forces such as radial and axial thrust, but the unsteady forces

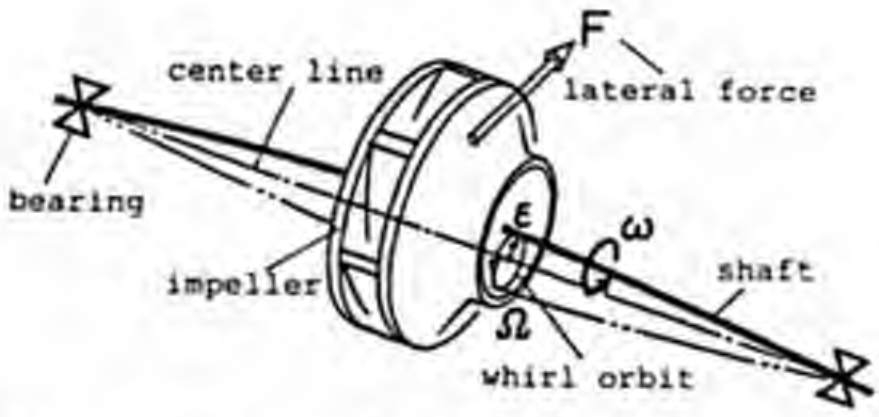

Fig. 15 Centrifugal impeller in whirl motion

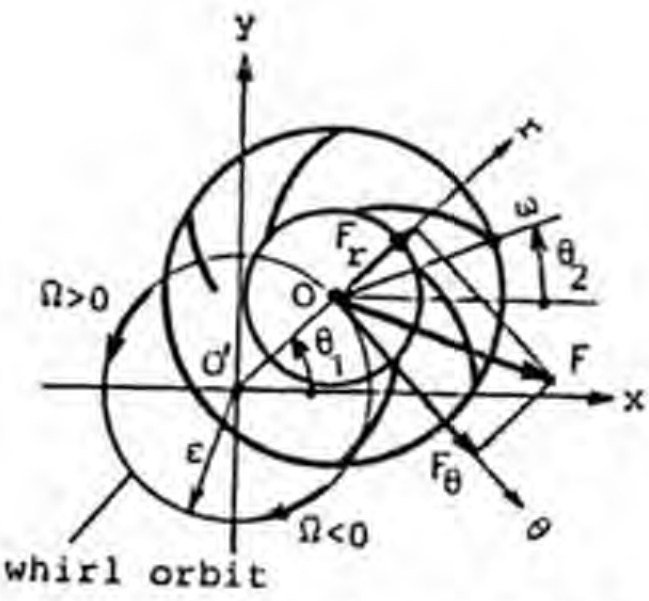

Fig. 16 Force components

which are induced directly by the oscillatory motion of the impeller. When a rotating shaft with a centrifugal impeller whirls as shown in Fig. 15, the impeller motion is the resultant of the whirl of the shaft center and the rotation of the shaft itself. The unsteady flow induced by this whirl motion applies a certain fluid force to the impeller. Since only forces normal to the shaft center give influence on the shaft vibration in a bending mode, our interests are also restricted to the normal component called lateral force.

In the current practice of rotordynamic analyses, a certain amount of fluid, usually the volume displaced by the impeller, is added to the impeller as apparent mass, so that only an assumed inertial centrifugal force is taken into consideration.

The bending mode vibration of a rotating shaft typically appears as a whirling motion with an elliptical orbit. If we consider the simple case of a circular orbit, the plane motion of the impeller is illustrated in Fig. 16. The impeller rotates counterclockwise with angular speed ω around its center O, which revolves with angular speed Ω around its absolute center O' along a circular orbit with eccentricity ε. Positive whirl occurs, when the shaft whirls in the same direction as its rotation, and negative whirl in the opposite direction.

The lateral fluid force on the impeller, F, is the one which is caused exclusively by the whirling motion. Therefore, any steady fluid forces, which may be caused either by azimuthally asymmetric configuration of surrounding casing or by misalignment of impeller center, are subtracted from the present consideration. The unsteady lateral force is further divided into radial and tangential components, F_r and F_θ, relative to the orbit as shown in Fig. 16.

The radial force component F_r applies a bending moment to the shaft and influences the natural frequency. The tangential force F_θ acts parallel to the motion of the shaft and thus transfers kinetic energy to the whirling rotor. In positive whirl, a positive F_θ (working opposite to the whirl motion) dissipates kinetic energy and exerts a stabilizing or damping effect, while a negative F_θ exerts a destabilizing or excitatory effect. In negative whirl these effects are reversed. When the tangential force becomes excitatory and feeds more kinetic energy to the whirling shaft than it damps out, a severe impeller-induced self-excitation or an impeller whip may occur. From the viewpoint of rotordynamic instability, tangential component has the primary significance.

In the absence of external forces, the whirl frequency is equal to the natural frequency of bending or critical speed of the shaft. Therefore, the case of whirl speed ratio $|\Omega/\omega| > 1$ corresponds to a subcritical, while $|\Omega/\omega| < 1$ to a supercritical rotational condition. When the shaft experi-

ences forced excitation due to an external force like a seismic load, the whirl frequency coincides with that of the external force. The whirl speed ratio Ω/ω, which should be covered in the study, must be determined from the above consideration.

Fluid Force Caused by Whirling Motion

In this section, the questions of why whirling fluid forces occur and how they are affected by whirl speed are answered by using a very simple model. Let us consider an impeller illustrated in Fig. 17 (a). It has only two small blades, A and B, and their fluid dynamic characters are approximated by those of an isolated airfoil. The figure shows the impeller geometry at the moment when absolute center O', impeller center O and two blades are aligned on a straight line, that is, x-axis in this case. This condition is not a singular one. For an impeller with a large number of blades, there are always a couple of blades, which are at the same disposition as that of the figure. The two blades considered in the model symbolize the ones which happen to be in such situation.

When there is no whirl, the lift on a blade, L_0, is proportional to the square of peripheral speed $u = R\omega$, where R is the radius of blade center, and its direction is normal to the relative inlet flow W as seen in the figure. If once whirl occurs, the impeller center O circles along the orbit with velocity $\varepsilon\Omega$. At the location shown in the figure the whole impeller moves upward with the same velocity, so that the absolute peripheral speed of blade A increases from u to $u+\varepsilon\Omega$, while that of B decreases from u to $u-\varepsilon\Omega$. Consequently the lift of blade A and B vary by $\pm\Delta L$, where ΔL is estimated by small perturbation principle as $\Delta L = 2L_0\varepsilon\Omega/u$.

The imbalance of lifts on blade A and B results in an impeller force F_L shown in Fig. 17 (b), which is proportional to whirl velocity $\varepsilon\Omega$. A body in an accelerative motion receives an inertial reaction from the surrounding fluid equivalent to apparent mass times acceleration. Let M_a be the apparent mass of impeller blades, the inertial force by whirl motion is $M_a\varepsilon\Omega^2$ to the direction normal to the orbit. This inertial force is indicated by F_M in the figure. The total fluid force F caused by the whirl motion is therefore the resultant of two force vectors, F_M and F_L. The radial and tangential components of force F is then written by

$$F_r = M_a\varepsilon\Omega^2 - k_r\varepsilon\Omega, \qquad F_\theta = k_\theta\varepsilon\Omega \qquad \text{.....(8)}$$

where k_r and k_θ are proportional constants.

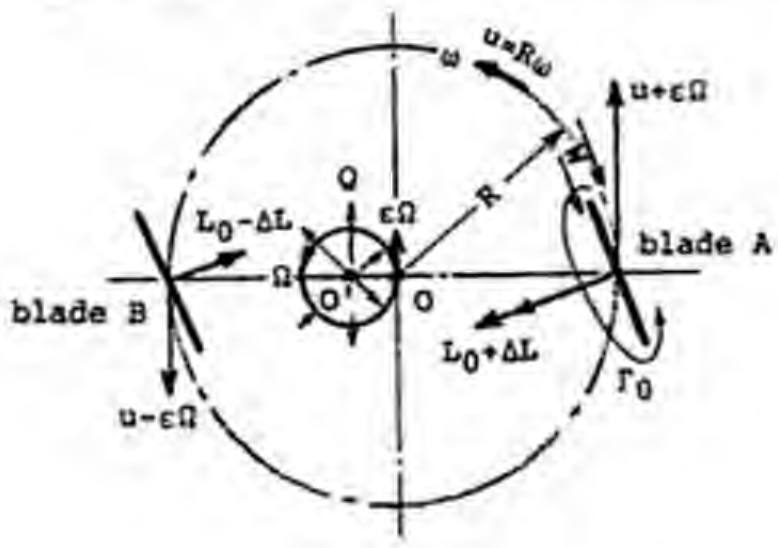

(a) Geometry

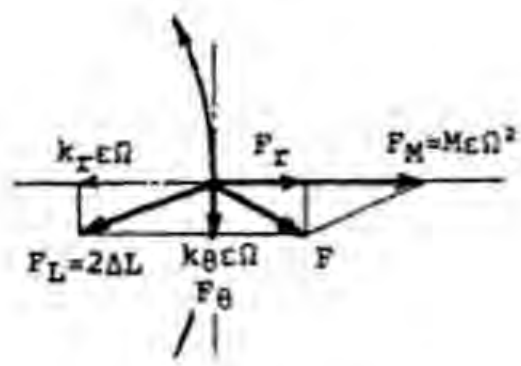

(b) Force

Fig. 17 Simple model of impeller force

The above analysis, though it is quite simple and qualitative, suggests the mechanism of whirling fluid force and also its relation to the whirl speed. As seen from Fig. 17 (a), the absolute center O', which represents the center of suction pipe and thus the location of source Q, changes its relative position to impeller blades during whirl. This induces a source-oriented perturbation on blades and results in a corresponding unsteady fluid force. This effect has, however, only a secondary significance as compared to the primary effect due to whirl speed-oriented perturbation.

Fluid Force on Whirling Centrifugal Impeller

Analytical and experimental studies have been conducted for centrifugal impellers of various configurations [Ref. 17-20]. In these experiments impellers are forced into whirl motion and the induced fluid forces are measured by load cells. Fig. 18 illustrates the layout of test facility used in the author's laboratory. It is virtually a single-stage vertical-shaft, centrifugal pump and the test impeller is forced to a circular orbital motion by the apparatus shown in Fig. 19 [Ref. 21]. Fluid forces can be separated from the measured total forces by subtracting inertial forces of the whirling impeller, which can be determined by whirl test in the air.

Fluid forces, radial as well as tangential, vary on the orbit due to an asymmetric discharge condition or to the impeller/guide vane interaction. Since the motion of a whirling rotor is governed by the impulse of the fluid force over an orbit, the force components, F_r and F_θ, are hereafter averaged over one cycle of whirl, and are denoted by $\bar{F}_r$ and $\bar{F}_\theta$. These forces are further normalized using the following definitions:

$$f_r = \bar{F}_r / M\varepsilon\omega^2, \quad f_\theta = \bar{F}_\theta / M\varepsilon\omega^2 \qquad \text{.....(9)}$$

$$M = \rho\pi r_2^2 b$$

where M denotes the reference mass and r_2=outer radius, b=exit width of the impeller.

Fig. 20 (a) and (b) show typical results obtained for a model impeller of boiler feed pump with vaned diffuser. The normalized radial and tangential forces are plotted against whirl speed ratio at design flow rate in

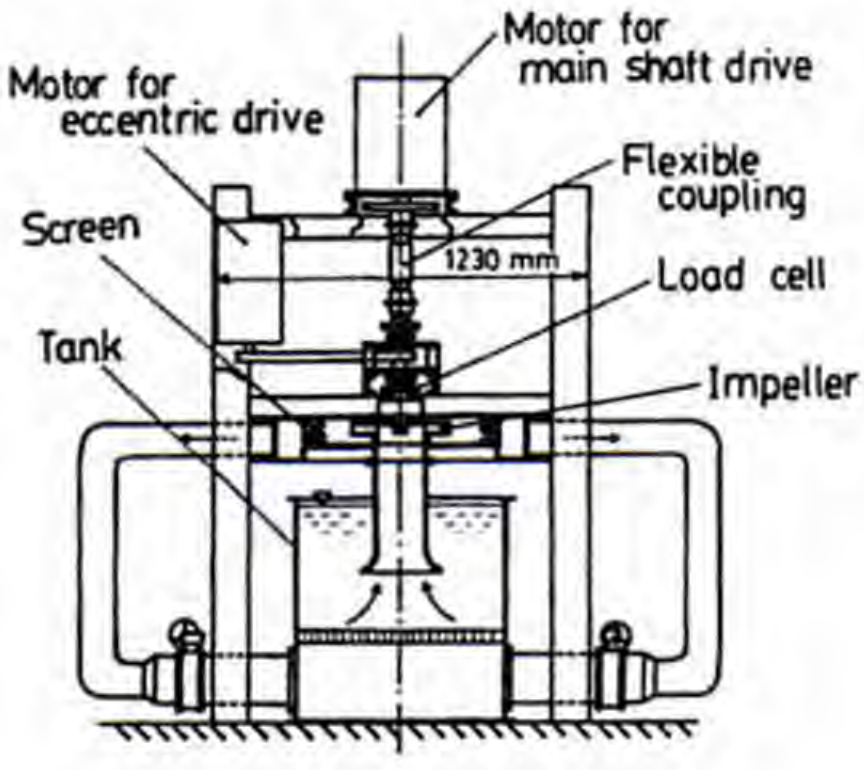

Fig. 18 Test setup

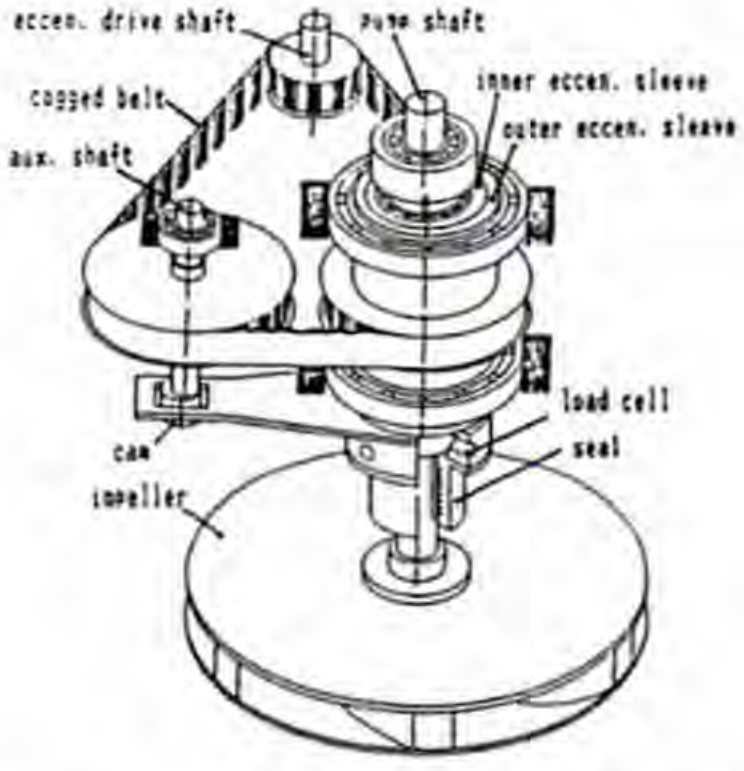

Fig. 19 Apparatus for forced whirl

(a) and at shut-off in (b). The fundamental tendency of the fluid forces agrees with the one predicted by a very simple model (cf. Eq.(8)). As seen from the comparison of these two figures, the behavior of whirling fluid forces becomes somewhat irregular at very low flow rate, where large separation develops in the impeller and diffuser.

Conversion to Force Matrices

For the vibration analysis of a rotor with centrifugal impellers, fluid forces must be formulated for an arbitrarily given motion of the shaft center. Although the experiment was conducted for a circular orbital motion, the results can be generalized to an arbitrary shaft motion, if the forces are assumed to be proportional to the displacement, velocity and acceleration of the shaft center. Using absolute coordinate system with its origin at the whirl center O' (cf. Fig. 16), x- and y-components of fluid forces, F_x and F_y, on impeller at O(x,y) are expressed by the following relation with three linear terms:

$$\begin{bmatrix} F_x \\ F_y \end{bmatrix} = -\underbrace{\begin{bmatrix} m_{xx} & m_{xy} \\ m_{yx} & m_{yy} \end{bmatrix}}_{\text{mass}} \begin{bmatrix} \ddot{x} \\ \ddot{y} \end{bmatrix} - \underbrace{\begin{bmatrix} b_{xx} & b_{xy} \\ b_{yx} & b_{yy} \end{bmatrix}}_{\text{damping}} \begin{bmatrix} \dot{x} \\ \dot{y} \end{bmatrix} - \underbrace{\begin{bmatrix} k_{xx} & k_{xy} \\ k_{yx} & k_{yy} \end{bmatrix}}_{\text{stiffness}} \begin{bmatrix} x \\ y \end{bmatrix} \quad .....(10)$$

where $x=\varepsilon\cos\theta_1$, $y=\varepsilon\sin\theta_1$ and $\theta_1=\Omega t$.

The assumption that the fluid forces are uniform and identical at every location on the orbit leads to the relations

$$\begin{aligned} F_r(\varepsilon,\Omega) &= \varepsilon\,(F_{r0} + F_{r1}\Omega + F_{r2}\Omega^2) \\ F_\theta(\varepsilon,\Omega) &= \varepsilon\,(F_{\theta 0} + F_{\theta 1}\Omega + F_{\theta 2}\Omega^2) \end{aligned} \quad .....(11)$$

The six constants in the above equations are related to twelve unknown elements in three force matrices of Eq.(10) by

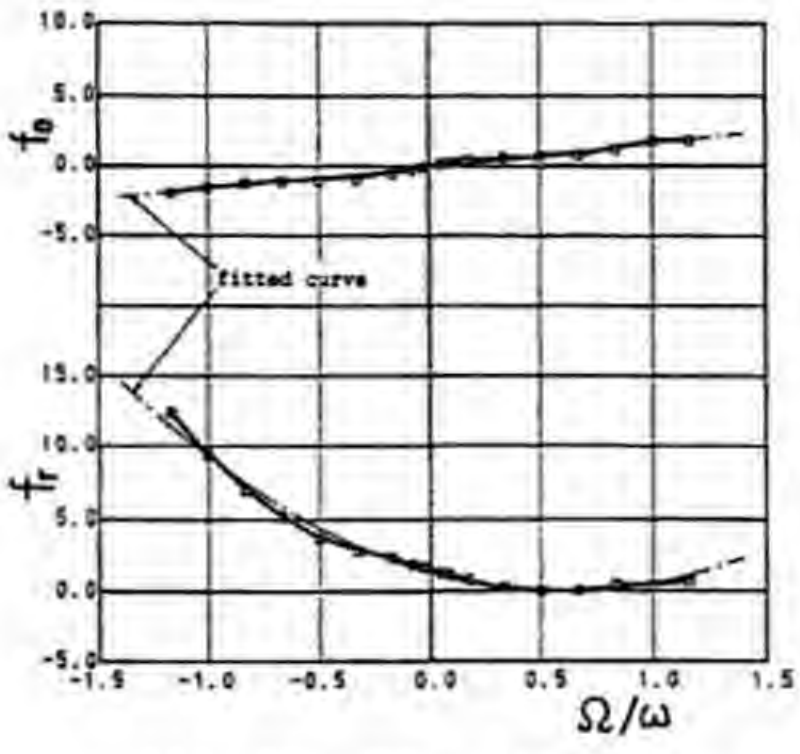

(a) At design flow rate

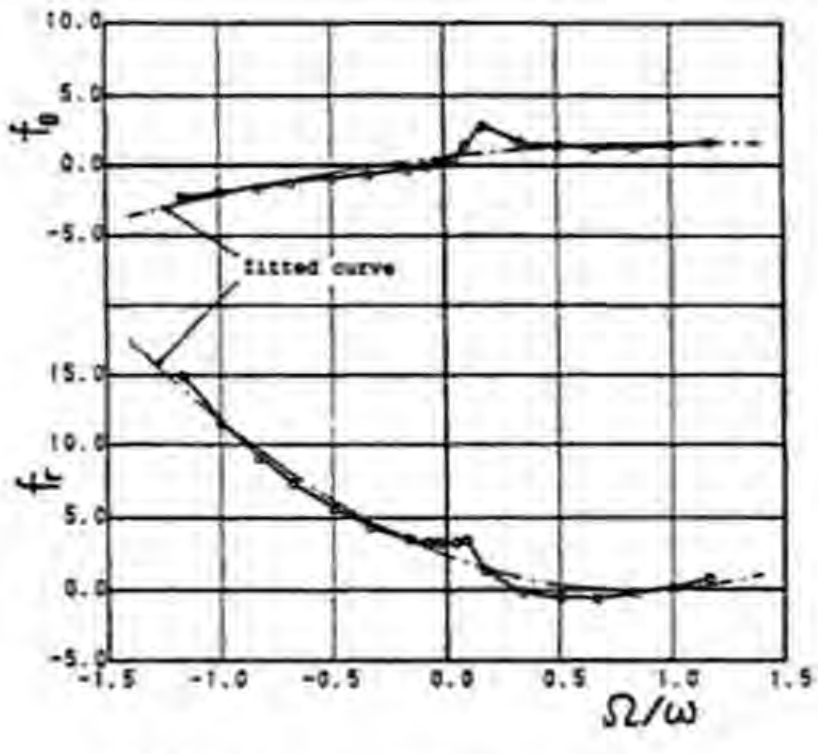

(b) At zero discharge

Fig. 20 Normalized fluid forces on whirling impeller

$$m_{xx} = m_{yy} = F_{r2}', \quad m_{xy} = -m_{yx} = F_{\theta 2}$$
$$b_{xx} = b_{yy} = F_{\theta 1}', \quad b_{xy} = -b_{yx} = -F_{r1} \qquad \text{.....(12)}$$
$$k_{xx} = k_{yy} = -F_{r0}', \quad k_{xy} = -k_{yx} = -F_{\theta 0}$$

All measured data over the entire whirl speed range are fitted to Eq. (12) and the six constants, F_{r0}, F_{r1}..., are determined by the method of least squares. The thin lines in Fig. 20 (a) and (b) indicate how the curves of Eq.(11) with the good fit of the constants can reproduce the real phenomena. As seen from these figures, the character of whirling fluid forces can be properly represented by the assumed linear relation at least for these cases. The matrix elements derived by the above procedure are listed in Table 2.

If once a linear relation is assumed, the measured results can be converted to a formulation, which is directly applicable to the rotordynamic analysis. However, it should not be forgotten that the peculiar behaviors of fluid forces observed at partial flow rate are all buried away at the price of the convenience.

Table 2 Matrix elements

matrix element	m_{xx}, m_{yy}	$m_{xy}, -m_{yx}$	b_{xx}, b_{yy}	$b_{xy}, -b_{yx}$	k_{xx}, k_{yy}	$k_{xy}, -k_{yx}$
normalized by	$\rho\pi r_2^2 b$		$\rho\pi r_2^2 bw$		$\rho\pi r_2^2 bw^2$	
ϕ/ϕ_{sf} = 1.4	3.78	-0.13	1.92	-3.83	-1.32	-0.05
1.0	3.67	-0.08	1.64	-4.41	-1.29	-0.10
0.6	3.91	0.89	0.95	-5.19	-1.34	0.64
0.2	3.92	1.54	1.73	-5.80	-2.01	0.97
0.0	3.54	0.83	1.86	-5.87	-2.39	0.60

CONCLUSIONS

Unsteady performance of turbomachines has the closest interface with the stability of hydraulic and mechanical system to which they belong. First, the dynamic characteristics of turbopumps are introduced and their relation to the dynamics of hydraulic system is discussed.

Then the importance of fluid forces on whirling impeller to the dynamics of rotating shaft is explained and the typical results are introduced. Through these two topics, the procedures are demonstrated, by which fluid dynamic results are converted to a formulation readily applicable to the stability analyses.

REFERENCES

1. Tsukamoto, H. and Ohashi, H., Transient Characteristics of a Centrifugal Pump During Starting Period, ASME J. Fluids Engineering, vol. 104, pp. 6-14, 1982.
2. Tsukamoto, H. et al., Transient Characteristics of a Centrifugal Pump During Stopping Period, ASME J. Fluids Engineering, vol. 108, pp. 392-399, 1986.
3. Kaneko, M. and Ohashi, H., Transient Characteristics of a Centrifugal Pump During Quick Change of Discharge, Trans. JSME, Ser. B, vol. 48, no. 426, pp. 229-237, 1982 (in Japanese).

4. Greitzer, E.M., The Stability of Pumping System -- The 1980 Freeman Scholar Lecture, ASME J. Fluids Engineering, vol. 103, pp. 193-242, 1981.
5. Anderson, D.A. et al., Response of Radial-Bladed Centrifugal Pump to Sinusoidal Disturbances for Non-Cavitating Flow, NASA TN D-6556, 1971.
6. Wagner, W., Dynamischer Auftrieb von Tragfluegeln, ZAMM, vol. 5, no.1, pp. 17, 1925.
7. Brennen, C.E. and Acosta, A., The Dynamic Transfer Function for a Cavitating Inducer, ASME J. Fluids Engineering, vol. 98, pp. 182-191, 1976.
8. Ng, S.L. and Brennen, C.E., Experiments on the Dynamic Behavior of Cavitating Pumps, ASME J. Fluids Engineering, vol. 100, pp. 166-176, 1978.
9. Brennen, C.E., Bubbly Flow Model for the Dynamic Characteristics of Cavitating Pumps, J. Fluid Mechanics, vol. 89, pp. 223-240, 1978.
10. Ohashi, H., Analytical and Experimental Study of Dynamic Characteristics of Turbopumps, NASA TN D-4298, 1968.
11. Ohashi, H., Study on Dynamic Characteristics of Turbopumps, Report 1-3, Trans. JSME, vol. 33, no. 255, pp. 1769-1799, 1967 (in Japanese).
12. Kawata, Y. et al., the Dynamic Behavior of a Centrifugal Pump at Partial Operation and Its Effect on the System Instability, Trans. JSME, Ser. B, vol. 52, no. 480, pp. 2947-2953, 1986 (in Japanese).
13. Kawata, Y. et al., Experimental Research on the Measurement of the Dynamic Behavior of Multistage Centrifugal Pump, Proc., IAHR Work Group on the Behavior of Hydraulic Machinery Under Steady Oscillatory Conditions, Lille, France, Sept. 1987.
14. Someya, T., Journal Bearing Databook, Springer, 1987.
15. Black, H.F., Effects of Hydraulic Forces in Annular Pressure Seals on the Vibration of Centrifugal Pump rotors, J. Mech. Eng. Sci., vol. 11, no. 2, pp. 206-213, 1969.
16. Childs, D. and Kim, C., Analysis and Testing for Rotordynamic Coefficients of Turbulent Annular Seals with Different, Directionally Homogeneous Surface-Roughness Treatment for Rotor and Stator Element, NASA CP 2338, pp. 313-340, 1984.
17. Shoji, H. and Ohashi, H., Lateral Fluid forces on Whirling Centrifugal Impeller (1st Report: Theory), ASME J. Fluids Engineering, vol. 109, pp. 94-99, 1987.
18. Ohashi, H. and Shoji, H., ditto (2nd Report: Experiment in Vaneless Diffuser), ditto, pp. 100-106.
19. Jery, B. et al., Hydrodynamic Impeller Stiffness, Damping and Inertia in the Rotordynamics of Centrifugal Flow Pumps, NASA CP 2338, pp. 137-160, 1984.
20. Franz, R.J. et al., On the Effect of Cavitation on the Radial Forces and Hydrodynamic Stiffness of a Centrifugal Pump, NASA CP 2443, pp. 493-502, 1986.
21. Ohashi, H. et al., Fluid Force Testing Machine for Whirling Centrifugal Impeller, Proc., International Conf. on Rotordynamics, IFToMM/JSME, Tokyo, pp. 643-648, 1986.